Fast numerical techniques for FE simulations in electrical capacitance tomography

M. Neumayer, T. Suppan, T. Bretterklieber and H. Wegleiter
Christian Doppler Laboratory for Measurement Systems for Harsh Operating Conditions, Institute of Electrical Measurement and Sensor Systems, Graz University of Technology, Graz, Austria, and

Colin Fox
Department of Physics, University of Otago, Dunedin, New Zealand

Received 14 January 2023
Revised 1 May 2023
Accepted 7 June 2023

Abstract

Purpose – Nonlinear solution approaches for inverse problems require fast simulation techniques for the underlying sensing problem. In this work, the authors investigate finite element (FE) based sensor simulations for the inverse problem of electrical capacitance tomography. Two known computational bottlenecks are the assembly of the FE equation system as well as the computation of the Jacobian. Here, existing computation techniques like adjoint field approaches require additional simulations. This paper aims to present fast numerical techniques for the sensor simulation and computations with the Jacobian matrix.

Design/methodology/approach – For the FE equation system, a solution strategy based on Green's functions is derived. Its relation to the solution of a standard FE formulation is discussed. A fast stiffness matrix assembly based on an eigenvector decomposition is shown. Based on the properties of the Green's functions, Jacobian operations are derived, which allow the computation of matrix vector products with the Jacobian for free, i.e. no additional solves are required. This is demonstrated by a Broyden–Fletcher–Goldfarb–Shanno-based image reconstruction algorithm.

Findings – MATLAB-based time measurements of the new methods show a significant acceleration for all calculation steps compared to reference implementations with standard methods. E.g. for the Jacobian operations, improvement factors of well over 100 could be found.

Originality/value – The paper shows new methods for solving known computational tasks for solving inverse problems. A particular advantage is the coherent derivation and elaboration of the results. The approaches can also be applicable to other inverse problems.

Keywords ECT, FE simulation, Green's function, Jacobian operations

Paper type Research paper

The financial support provided by the Austrian Federal Ministry for Digital and Economic Affairs, the National Foundation for Research, Technology and Development and the Christian Doppler Research Association is gratefully acknowledged.

COMPEL - The international journal for computation and mathematics in electrical and electronic engineering
Vol. 42 No. 5, 2023
pp. 1101-1112
Emerald Publishing Limited
0332-1649
DOI 10.1108/COMPEL-01-2023-0017

1. Introduction

The inverse problem of electrical capacitance tomography (ECT) is to determine the spatial relative dielectric permittivity distribution $\varepsilon_r(x, y)$ in a domain Ω_{ROI} (region of interest) based on capacitive measurements (Neumayer *et al.*, 2011, 2012). Figure 1 depicts a 2D scheme of an ECT sensor for process tomography, where the sensing principle is applied to monitor material distributions inside pipes or vessels. The region Ω_{ROI} is the interior of a nonconductive pipe/vessel. N_{elec} electrodes are attached to the outside of the tube. The measurements are given by the $M = N_{elec}(N_{elec}–1)$ inter electrode capacitances. To obtain these measurements, an alternating current voltage is applied to one electrode. This electrode is referred to as the active electrode. At the other electrodes, the displacement currents to ground are measured, which are proportional to the inter electrode capacitances. This process is repeated for each electrode. To improve the immunity against external influences, the sensor is shielded by a screen that is connected to the ground potential.

The solution of the inverse problem of ECT then requires a model for the description of the material distribution $\varepsilon_r(x, y)$ and a forward model for the simulation of the measurements (Kaipio and Somersalo, 2004). The domain within the shield is denoted by Ω. $\partial\Omega$ denotes its boundary, and Γ_i, $i = 1, \ldots, N_{elec}$, denotes the boundaries of the electrodes. The governing partial differential equation (PDE) for ECT within Ω is given by $\nabla\cdot(\varepsilon_r \nabla V) = 0$, where V is the electric scalar potential. In the sensor simulation, the PDE is solved according to the measurement process. The boundary conditions on all electrodes and the shield are of Dirichlet type with $V_{\Gamma_i} = V_0$ on the active electrode and $V = 0$ on all other boundaries. Given the solution V_i for the ith electrode being the active electrode, the measurements are evaluated by $q_{j,i} = \oint \varepsilon_r \vec{n} \cdot \nabla V_i d\Gamma_j$ ($j = 1,\ldots, N_{elec}$, $j \neq i$). The results of the integral evaluation are stored in the $N_{elec} \times N_{elec}$ matrix Q. Hence, the simulation of the measurement requires N_{elec} solving the PDE. Note that, actually, only $M/2$ independent measurements can be made due to the reciprocity property. Also, note that, we compute charges as simulated measurements, as we skip a normalization by V_0. Yet this is no issue for our further discussion. In measurement applications, a calibration is performed between the sensor and the simulation model. The calibration compensates for affine deviations between the sensor and the model (Neumayer *et al.*, 2011); hence, it comprises the strength of the excitation signal.

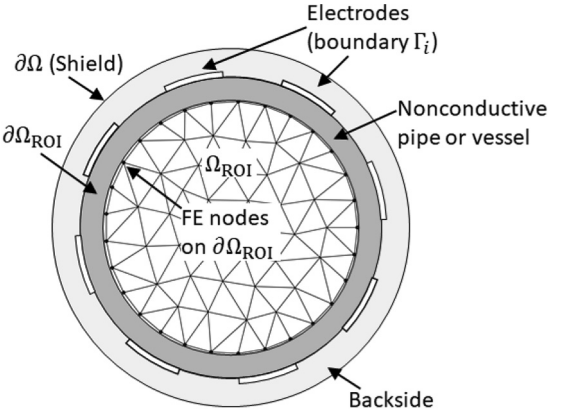

Figure 1.
Sketch of the elements of an ECT sensor in 2D

Source: Authors' own work

Throughout this work, we will use the finite element (FE) method for the simulation of the sensor and the description of the material distribution $\varepsilon_r(x, y)$. Following Figure 1, the spatial permittivity distribution $\varepsilon_r(x, y)$ is modeled by means of the FE discretization in Ω_{ROI} forming the vector $\varepsilon_r \in R^N$. The simulation of the sensor is given by the FE equation system:

$$\hat{K}(\varepsilon_r)V = R \tag{1}$$

where $\hat{K}(\varepsilon_r)$ is the symmetric $N_{FEM} \times N_{FEM}$ stiffness matrix. The $N_{FEM} \times N_{Elec}$ matrix R holds the right-hand side vectors for the excitation pattern of the measurements. For the incorporation of the boundary conditions in the matrix $\hat{K}(\varepsilon_r)$, we use the scheme of keeping the essential nodes (Ern and Guermond, 2004). The matrix V is of the same dimension as the matrix R, its column vectors hold the corresponding solution vectors for the scalar potential. Thus, equation (1) comprises all N_{Elec} solves. It is important to point out that the matrix $\hat{K}(\varepsilon_r)$ is linear with respect to the elements of ε_r due to the FE matrix assembly scheme (Ern and Guermond, 2004). The computation of Q is given by (Yan *et al.*, 1998):

$$Q = MV \tag{2}$$

where we refer to the sparse $N_{Elec} \times N_{FEM}$ matrix M as measurement matrix. Its nonzero coefficients represent the integral evaluation discussed in the previous paragraph. Note that equation (2) also provides the diagonal elements of Q. In our work, the matrix M is constant. So are the elements of $\hat{K}(\varepsilon_r)$ which represent the pipe and the backside of the ECT sensor.

Recent publications present a significant potential for the application of ECT technology for flow monitoring and mass flow metering in pneumatic conveying (Suppan *et al.*, 2021; Suppan *et al.*, 2019, 2022; Neumayer *et al.*, 2019a, 2019b, 2017). Also, applications in environmental sensing (Bretterklieber *et al.*, 2016; Flatscher *et al.*, 2017, 2015) and safety applications have been addressed (Fletcher, 1987). A prerequisite for these applications is the ability for fast numerical simulation techniques for the sensor. This does not only comprise the solution of equation (1) where the assembly of $\hat{K}(\varepsilon_r)$ is a known bottleneck but also computations involving the $M \times N$ Jacobian matrix $J = \left[\frac{\partial q_i}{\partial \varepsilon_{r,j}}\right]$ $(i = 1,\ldots, M, j = 1,\ldots, N)$. This is relevant for optimization based inverse problems methods, e.g. the gradient $g \in R^N$ of the objective function $\|q(\varepsilon_r) - q_{meas}\|_2^2$ can be evaluated by $g = J^T\Delta q$, with $\Delta q = q(\varepsilon_r) - q_{meas}$ being the residual vector (Neumayer *et al.*, 2019c). Here, $q \in R^M$ is a vector holding the measurements. In statistical inversion theory, the Jacobian is used as an approximation of the form $J\Delta\varepsilon_r$ to speed up Markov chain Monte Carlo methods (Watzenig *et al.*, 2011; Brandstatter, 2003).

The computation of the Jacobian has been addressed by several researchers. Two common techniques are the adjoint field method (Bradley, 2013; Brančík, 2004) and techniques based on the derivation of the stiffness matrix (Adler *et al.*, 2017; Young, 1988), whereby in (Young, 1988) also an equivalence between these methods is addressed. For the computation of the Jacobian using adjoint field methods, an additional equation system of the form of equation (1) has to be solved (Bradley, 2013). This makes the calculation of the Jacobi expensive, especially since we are interested in matrix vector products of the Jacobian or its transpose.

In this work, we present fast numerical techniques for the addressed computational bottlenecks. In particular, we will show that matrix vector products including the Jacobian

or its transpose can be computed for free, i.e. without any additional solves. The contributions and novelty of the paper are:

- a solution approach based on Green's functions;
- fast stiffness matrix assembly technique based on an eigenvector decomposition;
- Jacobian operations to evaluate $J\Delta\varepsilon_r$ and $J^T\Delta q$ without an explicit evaluation of the Jacobian; and
- demonstration of methods the within a BFGS (Broyden–Fletcher–Goldfarb–Shanno) based Gauss Newton scheme for deterministic inversion.

The methods include dedicated pre-processing steps as well as techniques, which are used during the solution of inverse problems. In the following sections, we address these points.

2. Solution with Green functions

In this section, we present the solution of equations (1) and (2) by a Green's functions approach and a modified charge computation scheme. Note that, the later scheme is not required but offers some further options, which we will address.

As depicted in Figure 1, only the material values in the domain Ω_{ROI} change. The properties (geometry and material values) of the domain $\overline{\Omega} = \Omega - \Omega_{\mathrm{ROI}}$ do not change. We therefore propose a charge computation scheme of the form:

$$Q = Q_{\overline{\Omega}} + M_{\partial\Omega_{\mathrm{ROI}}} V_{\partial\Omega_{\mathrm{ROI}}} \tag{3}$$

The computation of the charges is therefore based on potential of the $N_{\partial\Omega_{\mathrm{ROI}}}$ FE nodes on the boundary $\partial\Omega_{\mathrm{ROI}}$, which is the inner wall of the tube. The charge matrix $Q_{\overline{\Omega}}$ represents the "sensor backside." $Q_{\overline{\Omega}}$ has the same dimensions as the matrix Q, and $M_{\partial\Omega_{\mathrm{ROI}}}$ has the dimension of $N_{\mathrm{elec}} \times N_{\partial\Omega_{\mathrm{ROI}}}$. Both matrices can be determined numerically. For the determination of $Q_{\overline{\Omega}}$, a sensor simulation is performed, where the potential on $\partial\Omega_{\mathrm{ROI}}$ is set to zero. The elements of $M_{\partial\Omega_{\mathrm{ROI}}}$ are determined by simulations where the potential on each node is set to one, while all other nodes have the potential of zero. The addressed $N_{\partial\Omega_{\mathrm{ROI}}} + N_{\mathrm{elec}}$ computations are carried out in a preprocessing step.

Based on equation (3), the evaluation of Q now requires the evaluation of the potentials on $\partial\Omega_{\mathrm{ROI}}$, which are held in the matrix $V_{\partial\Omega_{\mathrm{ROI}}}$. Instead of assembling $V_{\partial\Omega_{\mathrm{ROI}}}$ from V by solving (1), we take advantage of the symmetry of $\hat{K}(\varepsilon_r)$, which allows the computation of $V_{\partial\Omega_{\mathrm{ROI}}}$ by:

$$\hat{K}(\varepsilon_r)G = E_{\partial\Omega_{\mathrm{ROI}}} \tag{4}$$

$$V_{\partial\Omega_{\mathrm{ROI}}} = G^T R \tag{5}$$

The $N_{\mathrm{FEM}} \times N_{\partial\Omega_{\mathrm{ROI}}}$ matrix $E_{\partial\Omega_{\mathrm{ROI}}}$ holds the identity vectors corresponding to the FE node numbers for the nodes on $\partial\Omega_{\mathrm{ROI}}$. The column vectors of G are referred to as Green's functions (Zhang and Fuzhen, 2005). From equation (5), it can be seen that Green's functions act as an" inverse operator", i.e. it can be used to replace $\hat{K}(\varepsilon_r)^{-1}$. This property will be used for the later addressed methods. Yet equation (4) has a significant disadvantage as $N_{\partial\Omega_{\mathrm{ROI}}}$ simulations are required. We therefore right multiply equation (4) with $M^T_{\partial\Omega_{\mathrm{ROI}}}$, which yields to:

$$\hat{K}(\varepsilon_r)\underbrace{GM^T_{\partial\Omega_{ROI}}}_{G_Q} = \underbrace{E_{\partial\Omega_{ROI}}M^T_{\partial\Omega_{ROI}}}_{R_Q} \tag{6}$$

and:

$$Q = Q_{\overline{\Omega}} + G_Q{}^T R \tag{7}$$

for the evaluation of the charges. Solving equation (6) for G_Q and computing the charges Q by (7) requires the same computational effort as the original problem, i.e. equations (1) and (2).

2.1 Comment on the choice of the charge computation

The evaluation of Q based on the potential $V_{\partial\Omega_{ROI}}$ as shown in equation (3) is based on the property that only the material within the domain Ω_{ROI} changes. Yet this choice for the charge computation is not unique. E.g. also from the nonzero columns of M in equation (2), a charge computation scheme can be derived. The Green's functions then have to be computed for the corresponding FE nodes, and the remaining scheme is the same as discussed above. However, we would like to point out that by using $V_{\partial\Omega_{ROI}}$ for the charge calculation, further possibilities for the solution of (6) arise. E.g. as only the block matrix corresponding to Ω_{ROI} within $\hat{K}(\varepsilon_r)$ changes, the Schur complement (Strang, 1986) might be used for its solution. We have not investigated this further in this work but want to make a note on it in relation to the choice of equation (3).

2.2 Properties of G_Q

The computation of G_Q in equation (6) offers significant advantages in conjunction with evaluations including the Jacobian matrix J. This will be addressed in Section 4 and is due to two properties:

(1) The Green's functions G_Q can be used to replace the product term $M_{\partial\Omega_{ROI}}\hat{K}(\varepsilon_r)^{-1}$; and

(2) For the FE nodes in Ω_{ROI}, the Green's functions G_Q equal the negative solution for the scalar potential V, i.e. $G_Q = -V$ holds in Ω_{ROI}.

The first property can be seen from equations (3) and (5).

The second property is less obvious but can be found from an analysis of the right-hand side matrices R and R_Q. For the sake of the length of this derivation, we want to show a numerical result here. Figure 2 depicts a 2D FE mesh of an ECT sensor with $N_{elec} = 16$ electrodes. The mesh has about 5,000 elements and about 3,000 FE nodes. The number of FEs in Ω_{ROI} (N) is about 700. The field plots in Figure 3 depict a column of V (left), G_Q (center) and the difference (V–G_Q) (right) for a 2D FEM simulation of an ECT sensor, respectively. For the FE nodes in Ω_{ROI}, the scalar potential V equals $-G_Q$. Hence, we can replace V by $-G_Q$ for computations involving the domain Ω_{ROI}. This will be shown in Section 4.1.

3. A fast matrix assembly scheme based on an eigenvector decomposition

A commonly known bottleneck in FE simulations is the assembly of the stiffness matrix. While this is less of an issue for single simulations, it can become a significant issue for the solution of inverse problems due to the required repeated simulation process. A well-known technique is to reduce the assembly effort by splitting $\hat{K}(\varepsilon_r)$ into a constant part and a variable part which is changed, e.g. as $\hat{K}(\varepsilon_r) = \hat{K}_{ini} + \wedge_{i=1}^{N}\varepsilon_{r,i}K_{e,i}$, where $K_{e,i}$ are the FE

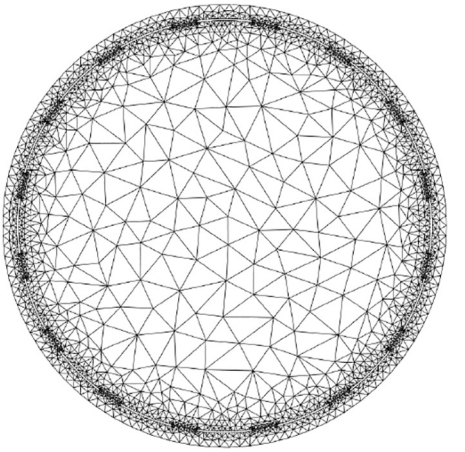

Figure 2.
2D FE mesh used for the numerical studies in this work

Source: Authors' own work

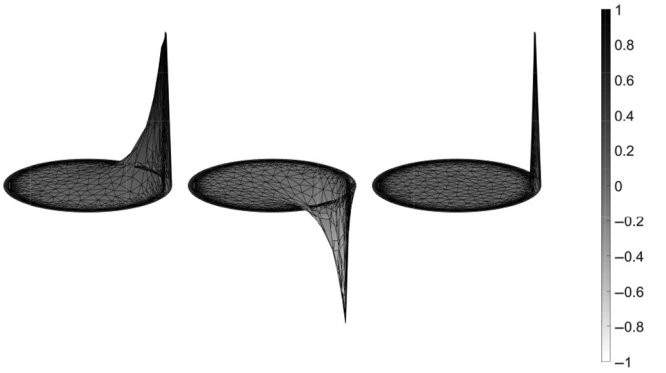

Figure 3.
Exemplary visualization of a column of V (left), GQ (center) and the difference V–GQ (right) for a 2D FEM simulation of an ECT sensor. Within the domain Ω_{ROI}, the solution V equals –GQ

Source: Authors' own work

element matrices. Here, the linearity of $\hat{K}(\varepsilon_{\mathrm{r}})$ with respect to the elements of ε_{r} can be seen. Yet the implementation of the update term can still remain a bottleneck, e.g. a loop type implementation without memory allocation is not suitable here.

Numerical linear algebra routines are highly efficient in the evaluation and storage of vector products of the form ab^T or matrix products of the form AB^T. Note that these products create matrices. For our further discussion, we use FEs of the order $p = 3$, i.e. the element matrices $K_{\mathrm{e},i}$ are of the form $K_{\mathrm{e}} = [k_{\mathrm{e},1}\ k_{\mathrm{e},2}\ k_{\mathrm{e},3}]$, where the vectors $k_{\mathrm{e},i}$ are its column vectors. Using these vectors, the element matrix can be expressed by $K_{\mathrm{e}} = \sum_{i=1}^{p} k_{\mathrm{e},i} e_i^T$.

We can expand this scheme by placing the column vectors $k_{\mathrm{e},i}$ within the sparse $N_{\mathrm{FE}} \times N$ matrices $\hat{K}_{\mathrm{e},i}$ such that the elements of $k_{\mathrm{e},i}$ appear at their global node number. Then the FE equation system can be assembled by:

$$\hat{K}(\varepsilon_r) = \hat{K}_{ini} + \sum_{i=1}^{p} \hat{K}_{e,i} \mathrm{diag}(\varepsilon_r) \hat{E}_{e,i}^T \tag{8}$$

where $\hat{E}_{e,i}$ hold the required identity vectors. This scheme, in conjunction with linear algebra routines, is already a highly efficient assembly technique for $\hat{K}(\varepsilon_r)$.

A further improvement can be obtained by exploiting the symmetry and positive semi-definiteness of the element matrices. For the exemplary case of $p = 3$, the eigen-decomposition provides:

$$K_e = \begin{bmatrix} v_1 & v_2 & v_3 \end{bmatrix} \begin{bmatrix} d_1 & & \\ & d_2 & \\ & & 0 \end{bmatrix} \begin{bmatrix} v_1^T \\ v_2^T \\ v_3^T \end{bmatrix} \tag{9}$$

$$= \begin{bmatrix} \sqrt{d_1} v_1 & \sqrt{d_2} v_2 \end{bmatrix} \begin{bmatrix} \sqrt{d_1} v_1^T \\ \sqrt{d_2} v_2^T \end{bmatrix} \tag{10}$$

where the vectors v_i are its eigenvectors and d_i are the corresponding positive eigenvalues. As one eigenvalue is zero, the decomposition can be written as:

$$K_e = \begin{bmatrix} \sqrt{d_1} v_1 & \sqrt{d_2} v_2 \end{bmatrix} \begin{bmatrix} \sqrt{d_1} v_1^T \\ \sqrt{d_2} v_2^T \end{bmatrix} \tag{11}$$

By defining $a_i = \sqrt{d_i} v_i$, we can therefore assembly K_e by $K_e = \sum_{i=1}^{p-1} a_i a_i^T$. Hence, at the cost of an eigenvector decomposition in the pre-processing phase, we can reduce the sum in the assembly process to $p - 1$, which corresponds to a reduction of one third for linear triangular elements.

By storing the vectors a_i in the $N_{FE} \times N$ matrices $\hat{A}_i$ as addressed before, the stiffness matrix assembly can be performed by:

$$\hat{K}(\varepsilon_r) = \hat{K}_{ini} + \sum_{i=1}^{p-1} \hat{A}_i \mathrm{diag}(\varepsilon_r) \hat{A}_i^T \tag{12}$$

The presented decomposition is known in literature as a $A^T CA$ decomposition (Hansen, 1998) that can be applied to equilibrium systems. Note that the transpose operation appears in the first matrix of the $A^T CA$ decomposition, whereas in our derivation it appears in the last matrix. For our derivation, this is due to the notation of the eigenvector decomposition. Here, a change of the transpose sign can be seen as a definition.

3.1 Timing measurements for equation (12)

To evaluate the performance, we performed timing measurements of our MATLAB implementation using MATLABs profiler function. For the FE mesh depicted in Figure 2, we achieved an average execution time for equation (12) of 58 μs on an AMD Ryzen 5 2500U processor. In contrast, a (naive) loop implementation lasted several 10 ms. The average

overall time to compute the charges is 9 ms. It should be noted that the presented calculation schemes also provide the possibility of parallelization.

4. Jacobian operations

In this section, we present the efficient evaluation of matrix vector products $J\Delta\varepsilon_r$ and $J^T\Delta q$, where J is the $M \times N$ Jacobian matrix.

4.1 Fast evaluation of $J\Delta\varepsilon_r$

We first study the derivation with the expression:

$$(\hat{K} + dK)(V + dV) = R \tag{13}$$

which expresses the deviation of the potential V by dV due to a change of the FE stiffness matrix $\hat{K}$ by dK. Here again, the linearity of $\hat{K}$ is applied. From the product $\hat{K}V + \hat{K}dV + dKV + dKdV = R$, we obtain:

$$\hat{K}dV + dKV = 0 \tag{14}$$

The differential change of the scalar potential is therefore:

$$dV = -\hat{K}^{-1}dKV \tag{15}$$

and due to equation (2), we can also write:

$$dQ = -M\hat{K}^{-1}d\hat{K}V \tag{16}$$

By this, a derivative of Q with respect to the $\varepsilon_{r,i}$ can be expressed by:

$$\frac{dQ}{d\varepsilon_{r,i}} = -M\hat{K}^{-1}\left[\frac{d\hat{K}}{d\varepsilon_{r,i}}\right]V \tag{17}$$

The elements of $\frac{dQ}{d\varepsilon_{r,i}}$ in equation (17) therefore provide the rows of the Jacobian J. $\left[\frac{d\hat{K}}{d\varepsilon_{r,i}}\right]$ gives the element matrix $\hat{K}_{e,i}$ of the corresponding FE. Note that $\left[\frac{d\hat{K}}{d\varepsilon_{r,i}}\right]$ has the same dimension as the original FE equation system. Due to the linearity, we can therefore express $J\Delta\varepsilon_r$ by

$$\mathrm{J}\Delta\ \varepsilon_r \mathrel{\hat{=}} \Delta\mathrm{Q} = -\mathrm{M}\hat{\mathrm{K}}^{-1}\left[\bigwedge_{i=1}^{N}\mathrm{K}_{e,i}\Delta\varepsilon_{r,i}\right]\mathrm{V} \tag{18}$$

Equation (18) provides a Jacobian operation, i.e. an evaluation of the matrix vector product without an explicit evaluation of J but at the cost of solving N_{elec} equation systems with the stiffness matrix $\hat{K}$. We can know take advantage of the properties of the Green's functions G_Q. The product $M\hat{K}^{-1}$ can be directly replaced by G_Q^T. Since $[\wedge_{i=1}^{N}\mathrm{K}_{e,i}\Delta\varepsilon_{r,i}]$only leads to matrix entries for the domain Ω_{ROI}, we can replace V by $-G_Q$. Thus, we obtain

$$\mathrm{J}\Delta\ \varepsilon_{\mathrm{r}} \mathrel{\hat{=}} \Delta\mathrm{Q} = \mathrm{G}_{Q}^{T}\left[\bigwedge_{i=1}^{N} \mathrm{K}_{\mathrm{e},i}\Delta\varepsilon_{\mathrm{r},i}\right]\mathrm{G}_{Q} \tag{19}$$

i.e. a Jacobian operation that can be directly computed from the solution of equation (6).

The inner $[\wedge_{i=1}^{N}\mathrm{K}_{\mathrm{e},i}\Delta\varepsilon_{\mathrm{r},i}]$matrix can be assembled by any desired scheme, yet because of its advantage, we propose the use of the eigenvector-based assembly technique addressed in Section 3, which leads to:

$$J\Delta\varepsilon_{\mathrm{r}} \mathrel{\hat{=}} \Delta Q = G_{Q}^{T}\left[\sum_{i=1}^{p-1} \hat{A}_i \mathrm{diag}(\Delta\varepsilon_{\mathrm{r}})\hat{A}_i^{T}\right] G_{Q} \tag{20}$$

4.2 Fast evaluation of $J^T\Delta q$

The derivation of a fast evaluation of $J^T\Delta q$ based on the use of the Green's function G_Q^T is unfortunately not as straight forward as the derivation of $J\Delta\varepsilon_{\mathrm{r}}$ shown in Section 4.1. The derivation is based on studying the transpose of equation (19) for the column vectors of the matrix V. Furthermore, a matrix decomposition for the form AB^T is required for the element matrices. This equals the discussion in Section 3. Because of the length, we will therefore only state the final result using the eigenvector-based stiffness matrix assembly. The evaluation of $J^T\Delta q$ can be performed by:

$$g = J^T\Delta q = \left(\sum_{i=1}^{p-1}\left(G_Q^T\hat{A}_i\right)^T \odot \left(\Delta Q G_Q^T\hat{A}_i\right)\right) \tag{21}$$

where $\odot$ denotes a row- and column-wise multiplication. The matrix ΔQ is assembled from the residual vector Δq following the measurement scheme. Elements of Q that are not used for measurements are set to zero. Hence also the matrix vector product $J^T\Delta q$ can be directly evaluated given G_Q, i.e. after the solution of equation (6).

4.3 Timing measurements for equations (20) and (21)

We again performed timing measurements for our implementation, where we achieved average execution times for equation (20) of 0.8 ms. The computation setup is the same as discussed in Section 3.1. We also performed timing measurements with a reference implementation of an adjoint field method (Bradley, 2013), which lasted about 350 ms. This comparison is not entirely fair, as the implementation of the reference method was not fully optimized. Yet it is relevant that the evaluation of equations (20) and (21) does not require any additional solves. We found a second comparison by comparing the evaluation of equation (20) against the evaluation of $J\Delta\varepsilon_{\mathrm{r}}$ when the Jacobian J is given. The evaluation of $J\Delta\varepsilon_{\mathrm{r}}$ last on average 0.2 ms. The factor of four between these times is in favor of equation (20), since it does not require an explicit evaluation of J. Timing tests for the evaluation of equation (21) lead to similar results.

5. Application of $J^T\Delta q$ within a Broyden–Fletcher–Goldfarb–Shanno based Gauss Newton scheme

The presented numerical techniques are intended to speed up the solution of inverse problems, i.e. the reconstruction of the material distribution ε_{r} from measurements q_{meas}. In

this section, we demonstrate this by means of an exemplary reconstruction example where we estimate ε_r using the deterministic approach:

$$\varepsilon_r^* = \arg\min_{\varepsilon_r} \left\| q(\varepsilon_r) - q_{\text{meas}} \right\|_2^2 + \alpha \varepsilon_r^T L^T L \varepsilon_r \tag{22}$$

The first term in the objective function fits the model against the measurement. The second term is a regularization term, which is necessary due to the ill-posed nature of the inverse problem. For the matrix L, we used as second order derivative operator, which leads to a smoothing of the reconstruction result (Neumayer *et al.*, 2011). The regularization parameter α was selected using the L-curve criterion (Hansen, 1998). For the solution of Adler *et al.* (2017), we use the Gauss–Newton method to compute a descent direction by $p_k = -H_k^{-1} g_k$, where H_k is the Hessian and g_k is the gradient of the objective function. Here, we use the BFGS approximation of the inverse Hessian (Neumayer *et al.*, 2019c). The algorithm is given by:

- evaluate the Newton direction $p_k = -H_k^{-1} g_k$;
- set $\varepsilon_{r,k+1} = \varepsilon_{r,k} + s p_k$ and set $s_k = s p_k$;
- compute $z_k = g(\varepsilon_{r,k+1}) - g(\varepsilon_{r,k+1})$; and
- evaluate $H_{k+1}^{-1} = H_k^{-1} + \frac{s_k^T z_k + z_k^T H_k^{-1} z_k}{\left(s_k^T z_k\right)^2} s_k s_k^T - \frac{H_k^{-1} z_k s_k^T + s_k z_k^T H_k^{-1}}{\left(s_k^T z_k\right)}$.

The gradient g_k is the sum of the gradient of $\|q(\varepsilon_r) - q_{\text{meas}}\|_2^2$ and the gradient of the regularization term. The first component is evaluated by equation (21), which requires one computation of the Green's functions G_Q. The gradient of the regularization term can be computed analytically. The variable s in the second step is a step-size parameter, which we set to a constant value. In addition, we clipped relative permittivities smaller than 1. Figure 4 shows an exemplary reconstruction result. The actual material distribution is two round objects with a relative permittivity of $\varepsilon_r = 3.5$. The background permittivity is $\varepsilon_r = 1$. The boundaries of the inclusions are marked by dashed lines. The reconstruction result looks typical for the used regularization term. Also, the estimated relative permittivity meets the true value. From timing measurements, we determined an average iteration rate in the range of 100 Hz, which corresponds to the previous timing measurements. The vast amount of computation time for this nonlinear reconstruction

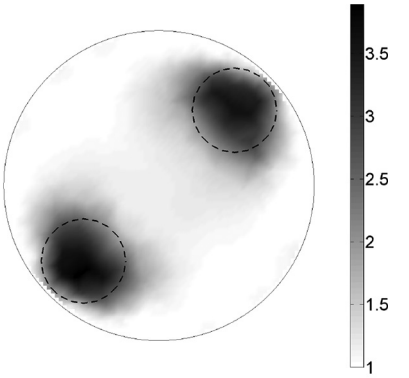

Figure 4.
Exemplary reconstruction of two rod type inclusions using the proposed BFGS-based algorithm

Source: Authors' own work

algorithm is reduced to the simulation of the sensor. The example shows the effectiveness of the methods, whereby the fast iteration rate is only one aspect for its application. Likewise, the methods offer the possibility to treat larger inverse problems.

6. Conclusion

In this work, we presented fast numerical techniques for FE simulations in ECT. We demonstrated a fast assembly technique for the FE equation system based on an eigenvector scheme as well as Jacobian operations. The techniques are based on the linearity of the problem and take advantage of a solution by Green's functions due to the symmetry of the FE stiffness matrix. Timing measurements showed the superior performance of the methods with respect to standard implementations. In fact, with the present approach, computations involving the Jacobian can be carried out for free, i.e. no additional effort is required as it is for known reference techniques like adjoint field methods. The techniques are applicable to other inverse problems and can also be used for different solution algorithms for inverse problems, like Kalman filters or inferential techniques. The well-structured notation of the calculations should allow researchers to easily integrate them into their own code.

References

Adler, A., Boyle, A. and Lionheart, W.R. (2017),"Efficient computations of the Jacobian matrix using different approaches are equivalent", in A. Boyle, R. Halter, E. Murphy and A. Adler, (Eds), *Proceedings of the 18th International Conference on Biomedical Applications of Electrical Impedance Tomography*, Thayer School of Engineering, Dartmouth, NH, USA, June 21-24, p. 75.

Bradley, A.M "Pde-constrained optimization and the Adjoint method", *Technical Report*. Stanford University, available at: https://cs.stanford.edu/ambrad. . ., Tech. Rep.

Brančík, L. (2004), "Comparative study of Jacobian calculation techniques in electrical impedance tomography", *Proceedings of VI. International Workshop" Computational Problems of Electrical Engineering*", Conference paper, p. 101.

Brandstatter, B. (2003), "Jacobian calculation for electrical impedance tomography based on the reciprocity principle", *IEEE Transactions on Magnetics*, Vol. 39 No. 3, pp. 1309-1312.

Bretterklieber, T., Neumayer, M., Flatscher, M., Becke, A. and Brasseur, G. (2016), "Model based monitoring of ice accretion on overhead power lines", *2016 IEEE International Instrumentation and Measurement Technology Conference Proceedings*, pp. 1-6.

Ern, A. and Guermond, J.-L. (2004), "Theory and practice of finite elements", 1st ed., *Ser. Applied Mathematical Sciences (Switzerland)*, No. 159. Springer.

Flatscher, M., Neumayer, M. and Bretterklieber, T. (2017), "Maintaining critical infrastructure under cold climate conditions: a versatile sensing and heating concept", *Sensors and Actuators A: Physical*, Vol. 267, pp. 538-546.

Flatscher, M., Neumayer, M., Bretterklieber, T., Moser, M.J. and Zangl, H. (2015), "De-icing system with integrated ice detection and temperature sensing for meteorological devices," in, *2015 IEEE Sensors Applications Symposium (SAS)*, pp. 1-6.

Fletcher, R. (1987), *Practical Methods of Optimization*, 2nd ed., Wiley-Interscience, New York, NY.

Hansen, P.C. (1998), *Rank-Deficient and Discrete Ill-Posed Problems: Numerical Aspects of Linear Inversion*, Society for Industrial and Applied Mathematics (SIAM), Philadelphia, PA.

Kaipio, J. and Somersalo, E. (2004), *Statistical and Computational Inverse Problems: v. 160*, 1st ed., ser. Applied Mathematical Sciences. Springer.

Neumayer, M., Steiner, G. and Watzenig, D. (2012), "Electrical capacitance tomography: current sensors/algorithms and future advances", *2012 IEEE International Instrumentation and Measurement Technology Conference Proceedings*, pp. 929-934.

Neumayer, M., Flatscher, M. and Bretterklieber, T. (2019b), "Coaxial probe for dielectric measurements of aerated pulverized materials", *IEEE Transactions on Instrumentation and Measurement*, Vol. 68 No. 5, pp. 1402-1411.

Neumayer, M., Suppan, T. and Bretterklieber, T. (2019c), "Statistical solution of inverse problems using a state reduction", *COMPEL – The International Journal for Computation and Mathematics in Electrical and Electronic Engineering*, Vol. 38 No. 5, pp. 1521-1532.

Neumayer, M., Bretterklieber, T., Flatscher, M. and Puttinger, S. (2017), "PCA based state reduction for inverse problems using prior information", *COMPEL – The International Journal for Computation and Mathematics in Electrical and Electronic Engineering*, Vol. 36 No. 5, pp. 1430-1441.

Neumayer, M., Zangl, H., Watzenig, D. and Fuchs, A. (2011), *New Developments and Applications in Sensing Technology, Ser. Lecture Notes in Electrical Engineering*, Springer, ch. Current Reconstruction Algorithms in Electrical Capacitance Tomography, Vol. 83, p. 337.

Neumayer, M., Suppan, T., Flatscher, M., Bretterklieber, T. and Stefan, P. (2019a), "Electrical capacitance tomography for monitoring of pneumatic conveying processes", *6. Tagung Innovation Messtechnik Tagungsband, 2019," Innovation Messtechnik", 40-Jahr-Jubliäum Hottinger Baldwin Wien*, 28-04-2009.

Schlegl, T., Bretterklieber, T., Neumayer, M. and Zangl, H. (2010), "A novel sensor fusion concept for distance measurement in automotive applications", *SENSORS, 2010, IEEE*, pp. 775-778.

Strang, G. (1986),*Introduction to Applied Mathematics*, Wellesley-Cambridge Press, Wellesley, MA.

Suppan, T., Neumayer, M., Bretterklieber, T. and Wegleiter, H. (2021), "Thermal drifts of capacitive flow meters: analysis of effects and model-based compensation", *IEEE Transactions on Instrumentation and Measurement*, Vol. 70 No. 70.

Suppan, T., Neumayer, M., Bretterklieber, T. and Stefan, P. (2019), "Prior design for tomographic volume fraction estimation in pneumatic conveying systems from capacitive data", *Transactions of the Institute of Measurement and Control*, Vol. 42 No. 4.

Suppan, T., Neumayer, M., Bretterklieber, T., Stefan, P. and Wegleiter, H. (2022), "A model-based analysis of capacitive flow metering for pneumatic conveying systems: a comparison between calibration-based and tomographic approaches", *Sensors*, Vol. 22 No. 3.

Watzenig, D., Neumayer, M. and Fox, C. (2011), "Accelerated Markov chain Monte Carlo sampling in electrical capacitance tomography", *COMPEL – The International Journal for Computation and Mathematics in Electrical and Electronic Engineering*, Vol. 30 No. 6, pp. 1842-1854.

Yan, H., Shao, F. and Wang, S. (1998), "Fast calculation of sensitivity distributions in capacitance tomography sensors", *Electronics Letters*, Vol. 34 No. 20, pp. 1936-1937.

Young, N. (1988), *An Introduction to Hilbert Space*, Cambridge University Press, New York, NY.

Zhang and Fuzhen (2005), *The Schur Complement and Its Applications*, Springer, New Haven.

Corresponding author
Markus Neumayer can be contacted at: neumayer@tugraz.at